ELSEVIER

Journal of Power Sources 111 (2002) 335–344

JOURNAL OF POWER SOURCES

www.elsevier.com/locate/jpowsour

Effect of surface treatment on electrochemical properties of $TiMn_{1.6}Ni_{0.4}$ alloy in alkaline electrolyte

K. Ramya[a], N. Rajalakshmi[a], P. Sridhar[a,*], B. Sivasankar[b]

[a]*Center for Energy Research, SPIC Science Foundation, 111 Mount Road, Guindy, Chennai 600032, India*
[b]*Department of Chemistry, Anna University, Guindy, Chennai 600025, India*

Received 3 April 2002; accepted 5 June 2002

Abstract

The characteristic features of the electrochemical behaviour of the treated hydrogen-storage alloy $TiMn_{1.6}Ni_{0.4}$ in an etching solution containing hydrogen fluoride and untreated alloy in alkaline media are investigated. Alloy characteristics such as discharge capacity, high-rate dischargebility and cycle-life are examined. The exchange current density, polarisation resistance and diffusion coefficients are also determined as functions of state-of-charge of the electrodes. The diffusion coefficient is found to be of the same order for the treated and the untreated alloy.

Keywords: Metal hydrides; AB_2 alloys; Electrochemical studies; Etching; Hydriding and dehydriding

1. Introduction

Metal hydrides are currently being investigated as alternative materials to the cadmium electrode of Ni–Cd batteries because of their high specific energy, longer life, and environmental acceptability. Several metal hydrides based on AB_2 and AB_5 type alloys have been developed as negative electrode materials in nickel–metal hydride (Ni–MH) batteries [1–7]. Among these, titanium-based metal hydrides are promising materials for negative electrodes because their gravimetric hydrogen-storage capacities are higher than those of zirconium-, lanthanum- and mischmetal (Mm)-based metal hydrides. Metal hydride alloy electrodes based on AB_2 type alloys have several shortcomings, such as slow activation owing to the formation of an oxide film on the surface of the alloy, poor rate capability, high self-discharge, high corrosion rate, and short cycle-life. Various modifications such as change in alloy composition and surface treatment have been investigated to overcome these shortcomings.

The effect of partial substitution and anodic oxidation treatment of Zr–V–Ni alloys on the electrochemical properties have been investigated by Wakao et al. [8]. Anodic oxidation treatment at −0.6 V versus Hg/HgO for the alloy is effective for electrode activation due to a change in surface structure from a hydrogen impermeable to a permeable state. Formation of an active nickel cluster on the surface contributes to activation. A sufficient amount of oxidation is attained by long-time immersion. Immersion at higher temperature shortens the time for activation by increasing the corrosion current.

Hot alkaline treatment of multiphase $Zr_{0.5}Ti_{0.5}V_{0.75}Ni_{1.25}$ alloy by Yan et al. [9] resulted in significant surface corrosion, with some corrosion products being soluble in the treatment solution. The corrosion process generated hydrogen which was largely absorbed by the alloy during treatment and resulted in heterogeneous particle cracking and significant electrochemical discharge capacity even before the first deliberate charge. The hot alkaline treatment is known to offer better activation of the alloy and offer benefit to cycle-life. The effect of alkaline solution on the surface oxide layers of the ZrTiNi alloy with La and Ti substitution has been studied by Kim et al. [10]. They found that La-based alloy is activated more than titanium-based alloy as titanium oxide is denser than lanthanum oxide. Activation of the alloy was thus found to depend on the nature of the oxide layer formed.

Choi et al. [11] have investigated the effect immersing Zr-based alloy in boiling 6 M KOH solution for varying periods of time. With increase in immersion period the charge–discharge characteristics of the alloy electrode greatly improved in alkaline solution. These effects were

* Corresponding author.
E-mail address: cerssf@md5.vsnl.net.in (P. Sridhar).

0378-7753/02/$ – see front matter
PII: S0378-7753(02)00338-5

attributed to a change in chemical composition of the surface and bulk of the alloy. Yan and Suda [12] have investigated the electrochemical characteristics of $LaNi_{4.7}Al_{0.3}$ alloy treated with an alkaline solution containing hydrazine ($N_2H_4{\cdot}H_2O$) under various treatment conditions. They found that hydrazine solution could activate the alloy to attain a high initial discharge capacity at fast charge and discharge rates and at low polarisation. The strong reducing agent N_2H_4 is beneficial in terms of high catalytic activity.

Zuttel et al. [13] have studied the influence of pretreatment of the metal hydride powder $Zr(V_{0.25}Ni_{0.75})_2$ with KOH and fluoride containing solutions on the surface composition of the alloy grains by X-ray photoelectron spectroscopy (XPS). A relationship between the surface composition of the hydrogen storing alloy and the electrode performance was established. The speed of activation increased with increasing nickel content in the top surface layers of the metal hydride. Surface treatment of Zr-based alloy by ultrasound treatment in $KF + KH_2PO_2$ solution also improved the characteristics due to nickel-rich surfaces. The treated alloy showed easier activation, better high-rate discharge, higher exchange current density, and lower polarisation resistance [14] compared with untreated alloy.

Ciureanu et al. [15] have studied the electrochemical behaviour of amorphous $Ni_{64}Zr_{36}$ alloy in alkaline media. The changes occurring in both the physical state and composition of the surface layer during chemical etching and electrochemical activation were examined. The charge-acceptance of the alloy was found to be increased by chemical etching.

Although, data have been published on the effects of surface modification of alloys, the effect of these treatments on the cycle-life of the alloy and electrochemical parameters is considered to be useful. This investigation aims to identify the effect of etching on the electrochemical characteristics of metal hydride alloys, including the kinetics of charge-transfer and diffusion during the hydriding–dehydriding process as well as their cyclic-life performance.

2. Experimental

Alloy of the composition $TiMn_{1.6}Ni_{0.4}$ was prepared by arc melting. Care was taken to avoid metal evaporation as Mn is a low melting metal compared with Ti and Ni. Repeated turning and melting of the alloy ingots five times ensured homogeneity. To prepare the metal hydride electrodes, the alloy $TiMn_{1.6}Ni_{0.4}$ was first crushed and ground mechanically. The resultant powder was sieved through a mesh, which gave particles with a size of 75 μm. Etching of the alloy powder was carried out by immersion in a solution of $HF:H_2O_2:H_2O$ (1:1:30).

Electrodes were prepared by mixing the alloy powder and copper powder in a weight ratio of 1:3 with binder, followed by pressing the material on to a nickel mesh of area 1 cm^2. The electrode was immersed in a three-electrode test cell filled with 6 M KOH solution. Charge–discharge characteristics and cyclic voltammograms were obtained at 30 °C using EG&G Princeton Applied Research Potentiostat/galvanostat model 273 equipment. The electrode was charged at constant current until the hydrogen content reached its saturated value (as observed by H_2 evolution at the electrode). The potentials were measured against a saturated calomel electrode (SCE). All potentials are reported with respect to this electrode. The electrodes were discharged to a potential of −0.4 V. In order to obtain the diffusion coefficient of hydrogen, the activated electrode was discharged at a constant potential of −0.3 V.

3. Results and discussion

The object of etching treatment was to achieve an electrochemically active surface with good charge-acceptance. Etching does not remove the oxide layer from the surface. Etching makes the layer more porous and, hence, more permeable for hydrogen penetration during electrolytic charging.

Typical discharge curves of the etched and untreated $TiMn_{1.6}Ni_{0.4}$ alloy electrodes are given in Fig. 1. Initially, a potential plateau is observed and after a certain period of time, a drastic potential change occurs due to the depletion of hydrogen atoms from the electrode surface. The equilibrium potentials for the etched and untreated alloy electrodes are the same. This shows that the potential is independent of the treatment performed on the alloy, and is dependent only on the hydrogen content in the alloy. The etched sample has higher electrochemical hydrogen-storage capacity than the untreated sample. A maximum capacity of 615 mAh g^{-1} was obtained for the etched sample, while for the untreated electrode the maximum capacity was 514 mAh g^{-1}.

The change in discharge capacity of the untreated and etched alloy as a function of discharge current is shown in Fig. 2. The discharge capacity decreases with increase in discharge current. The capacity for the etched alloy electrode and the untreated alloy electrode are 561 and 414 mAh g^{-1}, respectively at a discharge current of 2000 mA g^{-1}. Discharge at high currents results in a capacity decrease of 9% for the etched alloy electrode compared with 19.5% for the untreated alloy electrode. This shows that the alloy can be discharged at high currents without appreciable loss in capacity.

The cycle-life of the etched alloy and untreated alloy is presented in Fig. 3. The activation cycle required for the etched alloy is lower in comparison with the untreated alloy since the maximum capacity for the etched alloy is obtained after 107 cycles, but after 134 cycles for the untreated alloy. These results can be attributed to the porous structure of the oxide layer which covers the alloy particles. The etched alloy has a surface permeable for hydrogen penetration due to its porous nature which increases the kinetics of hydrogen absorption. The porous structure of the electrode also results

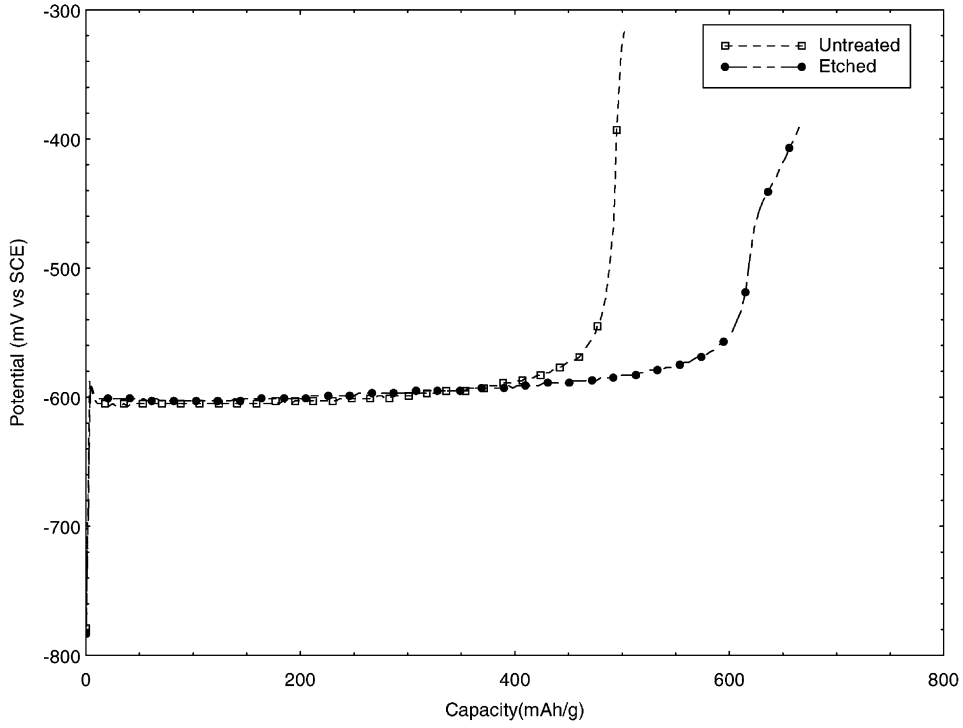

Fig. 1. Typical discharge curves for etched and untreated alloy.

in corrosion of the metal hydride alloy particles as it allows better contact with the alkaline KOH solution used as the electrolyte. Hence, a decrease in capacity is observed after maximum capacity is reached for the etched alloy electrode. Extensive corrosion leads to a decrease in capacity to 350 mAh g^{-1} after 175 cycles (a loss of about 45% in discharge capacity). The untreated sample, due to its protection by the oxide layer, takes longer time to become activated and the capacity after 190 cycles is 497 mAh g^{-1} (a loss of about 3.2% in discharge capacity). The cycle-life

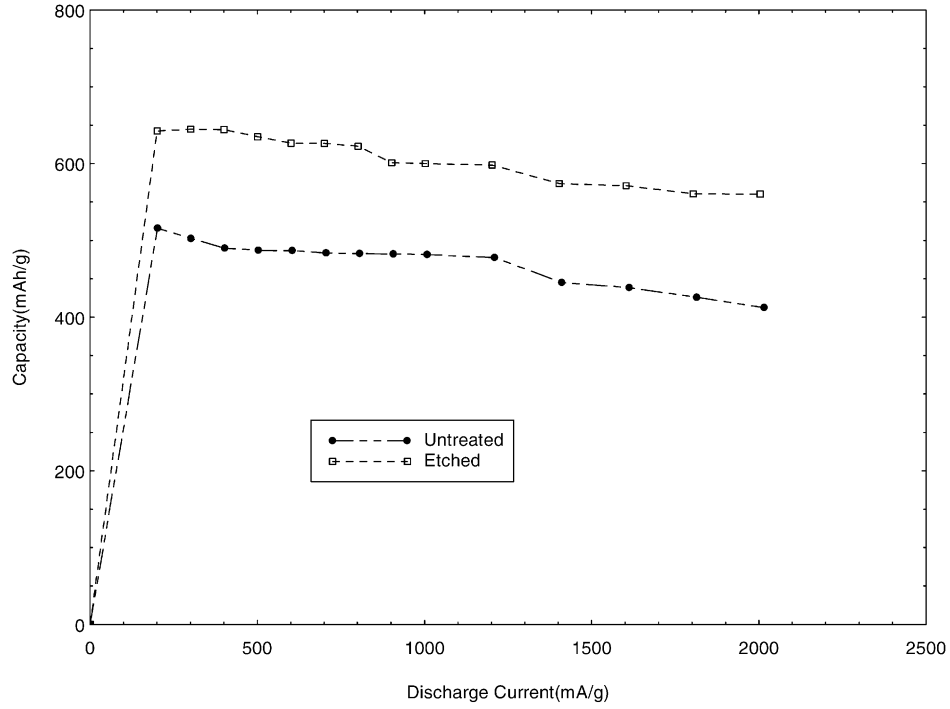

Fig. 2. Discharge capacity vs. discharge current curves for untreated and etched alloy.

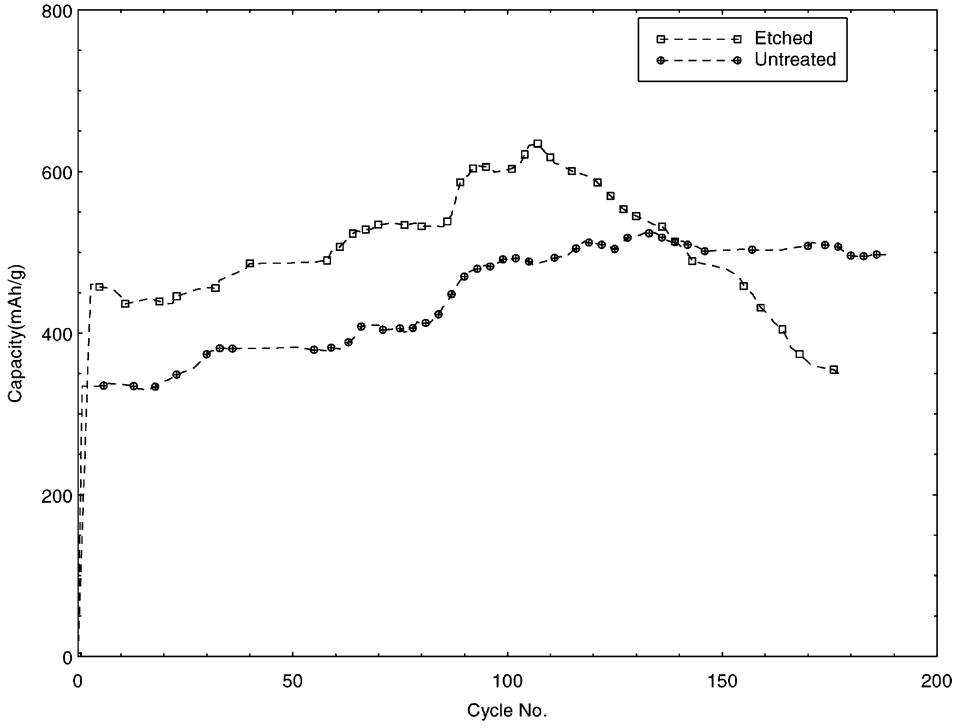

Fig. 3. Cycle-life curves for untreated and etched alloy.

characteristics of $TiMn_{1.6}Ni_{0.4}$ alloy thus indicates that although higher capacities can be achieved on etching, better durabilities are obtained only with untreated alloy electrodes.

Cyclic voltammograms at various sweep rates for the untreated $TiMn_{1.6}Ni_{0.4}$ alloy are shown in Fig. 4. At higher sweep rates, higher currents are obtained. At low sweep rates, there is sufficient time for reaching a steady-state due

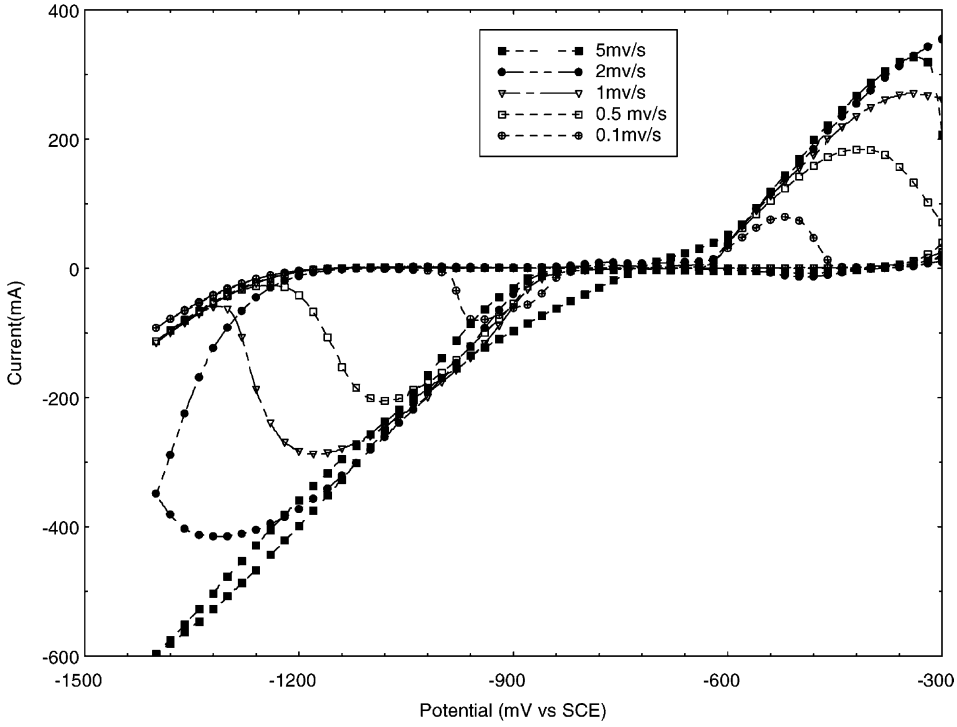

Fig. 4. Cyclic voltammograms for untreated $TiMn_{1.6}Ni_{0.4}$ ally at various scan rates.

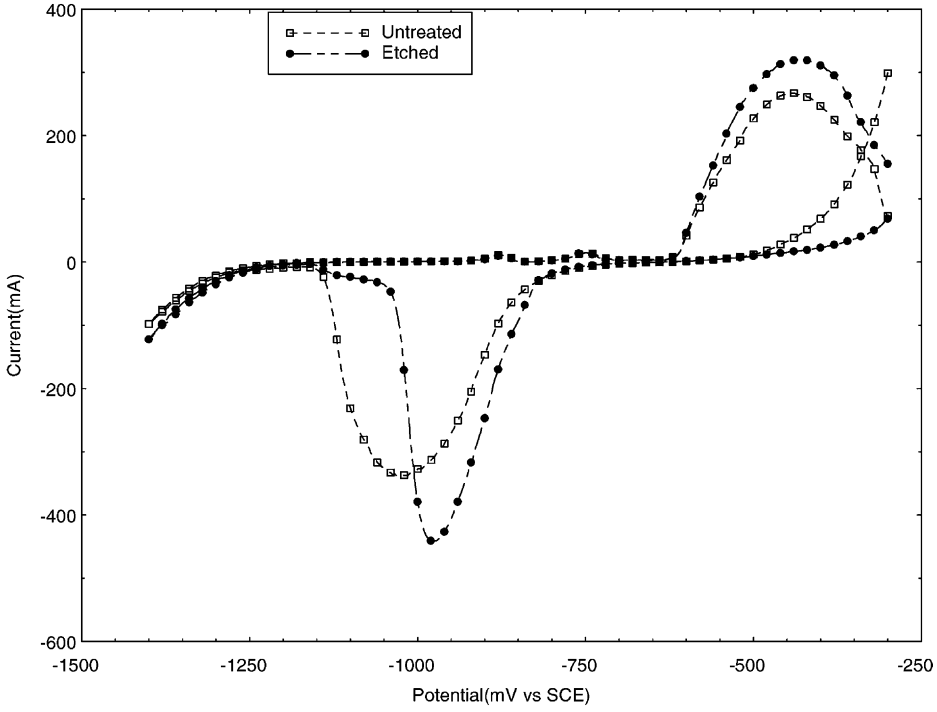

Fig. 5. Cyclic voltammograms for untreated and etched alloy.

to diffusion of the species from the bulk. Hence, a lower concentration gradient and a lower current are obtained. Also, prominent charging and discharging peaks are obtained. For higher scan rates, a high concentration gradient (as diffusion process is not allowed to set in), hence, a higher current is observed. The charging capacity (around 150 cycles) at 0.1, 0.5, 1 and 2 mV/s is 524.4, 521.2, 480.7 and 407.7 mAh g^{-1}, respectively.

The cyclic voltammograms for untreated and etched $TiMn_{1.6}Ni_{0.4}$ alloy at a scan rate of 1 mV s^{-1} are presented in Fig. 5. The charging capacity of the etched alloy is higher than the untreated alloy at the 75th cycle. The charging

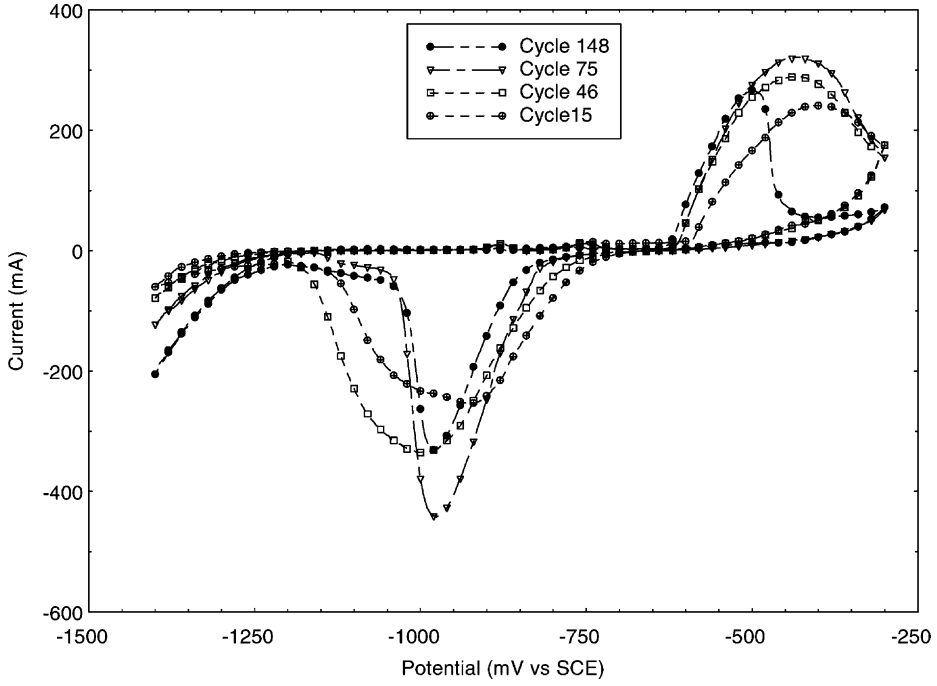

Fig. 6. Cyclic voltammograms for the etched alloy at various cycle numbers.

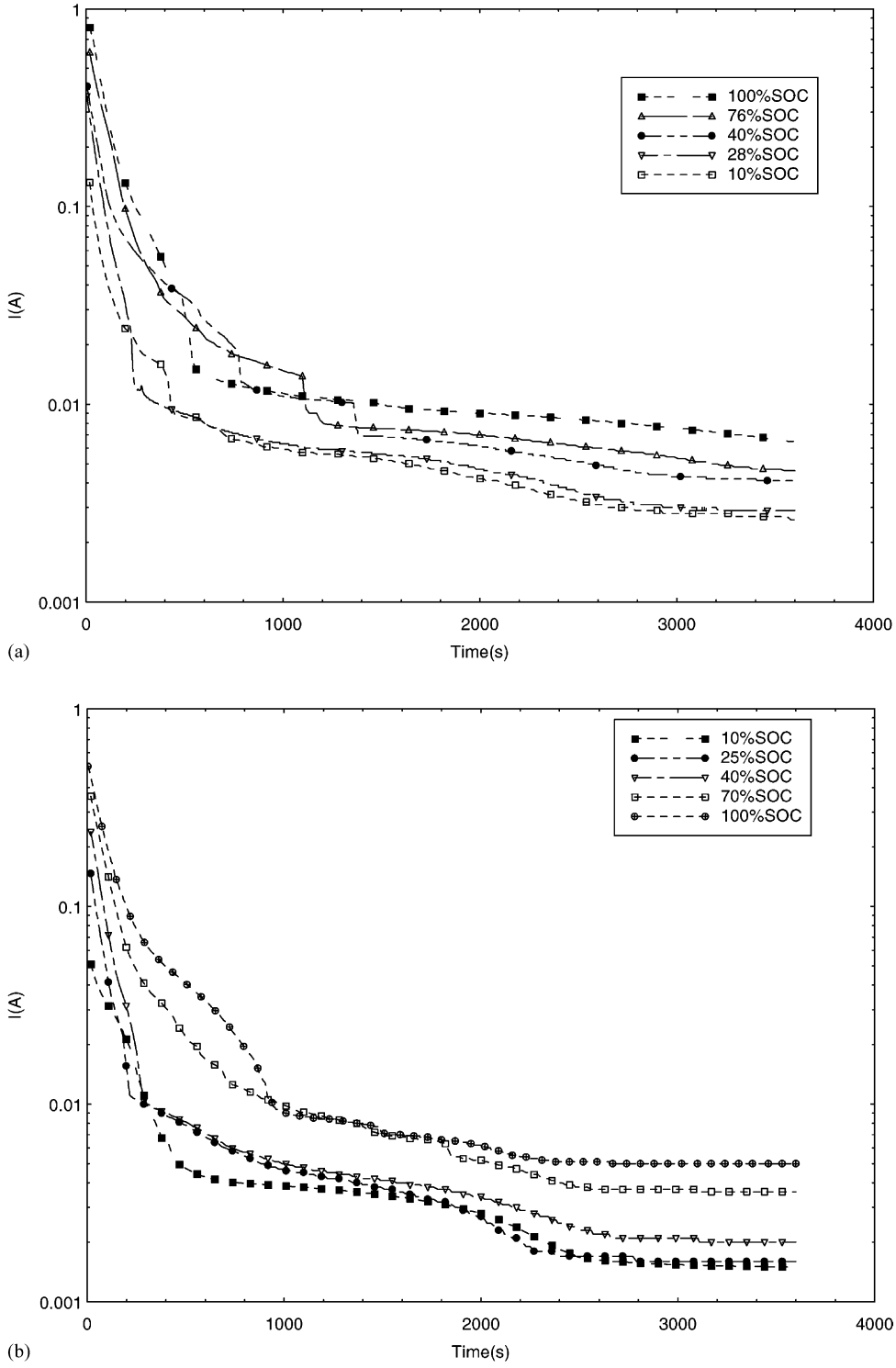

Fig. 7. Constant potential discharge curves for: (a) etched; and (b) untreated alloy at various states-of-charge.

capacity of the etched alloy is 405 mAh g^{-1} while that of untreated alloy is 389.7 mAh g^{-1}. The higher anodic peak current and the larger peak area in the voltammogram for the etched alloy clearly indicate higher activation than the untreated alloy. Curves at various cycles are given in Fig. 6. At the 15th cycle, the sample is not activated and has a capacity of 361.1 mAh g^{-1}. At the 46th cycle, the charging capacity is 405 mAh g^{-1}, while at the 75th cycle the capacity is 430 mAh g^{-1}. This indicates the activation of the alloy during cycling. The capacity at 145th cycle is 248.2 mAh g^{-1} which indicates a decrease in capacity due to extensive corrosion of the sample.

The controlled potential discharge curves at various states-of-charge for the etched and untreated alloy are shown

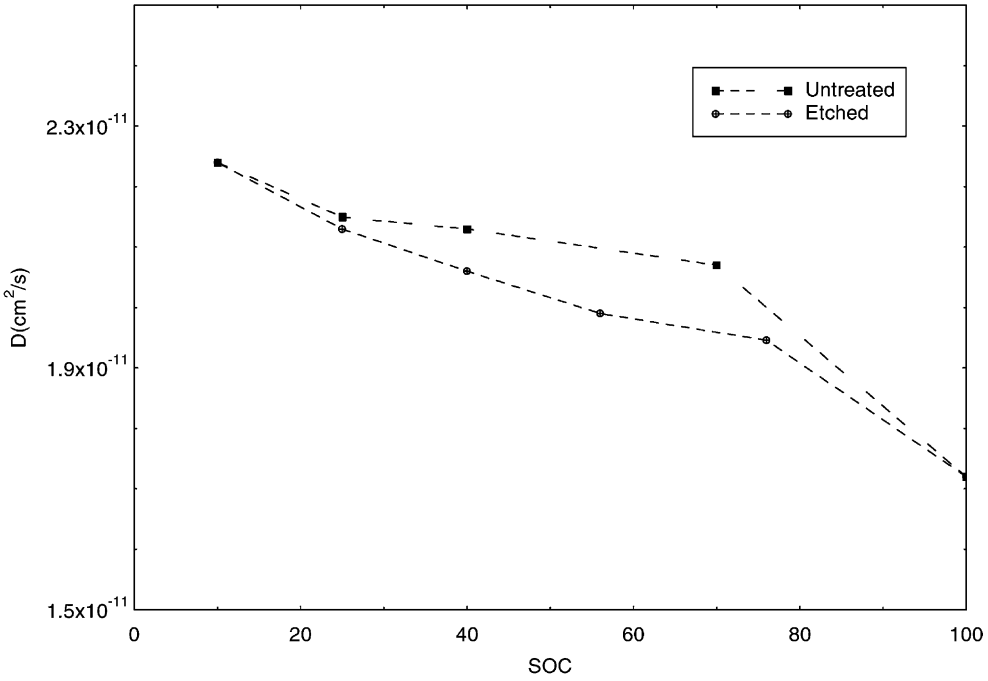

Fig. 8. Diffusion coefficient vs. state-of-charge for etched and untreated alloy.

in Fig. 7(a) and (b), respectively. During discharge, adsorbed hydrogen atoms are electrochemically oxidised. With decreasing surface concentration of the adsorbed hydrogen atoms during discharge, the hydrogen atoms in the alloy diffuse towards the surface at a velocity proportional to their concentration gradient. For a constant hydrogen surface concentration, the diffusion current (I) versus time (t) has been shown by Zheng et al. [16] to be:

$$\mathrm{Log}(I_t) = \pm \log\left[\frac{6FD(C_o - C_s)}{da^2}\right] - \frac{\Pi^2}{2.303} \times \frac{D}{a^2} \times t \qquad (1)$$

where C_o is the concentration in the bulk of the alloy, C_s a constant surface concentration, t the time, d is the density of the alloy, the $\pm$ sign indicates the charge ($-$) and discharge ($+$) process, a is the sphere radius of the alloy particle. From the slope of the linear portion of the curve between log I and time, the ratio D/a^2 can be obtained.

From Fig. 7(a) and (b), it can be seen that the value of Log I immediately decreases after a potential step. It also decreases with decrease in concentration of adsorbed hydrogen on the electrode surface due to electro-oxidation. The value thereafter decreases linearly, according to Eq. (1), because the rate-determining step changes from electro-oxidation to hydrogen diffusion in alloy. The Fick's diffusion coefficient, D, was calculated from the slope of the plot at large times, and has been plotted in Fig. 8. The average value of the diffusion coefficient for untreated and etched alloys is 2.06×10^{-11} and 2.01×10^{-11} cm^2 s^{-1}, respectively. This shows that the hydrogen diffusion behaviour does not change with surface modifications in the alloy.

3.1. Electrochemical kinetics of hydrogen absorption and desorption

The kinetics of hydrogen absorption and desorption are dependent on the surface properties of the alloy particles. To quantify the effect of surface treatment on the kinetics, dc polarisation and ac impedance experiments were performed on the untreated and surface-etched alloy electrodes. Polarisation experiments were performed on the electrodes under potentiodynamic conditions at a scan rate of 1 mV s^{-1}. Typical polarisation curves for the untreated and etched alloy electrodes at different states-of-charge are presented in Fig. 9(a) and (b), respectively. The exchange current density was calculated using the following equation:

$$i = \frac{i_0 F \eta}{RT} \qquad (2)$$

where i is the current density, i_0 the exchange current density, F the Faraday constant, η the overpotential, R the

Table 1
Exchange current density (mA cm^{-2}) from the dc polarisation method

State-of-charge	For untreated alloy	For etched alloy
100	61.2	84.7
75	56.1	75.8
50	41.6	66.1
25	30.3	48.4
10	27.5	34.9

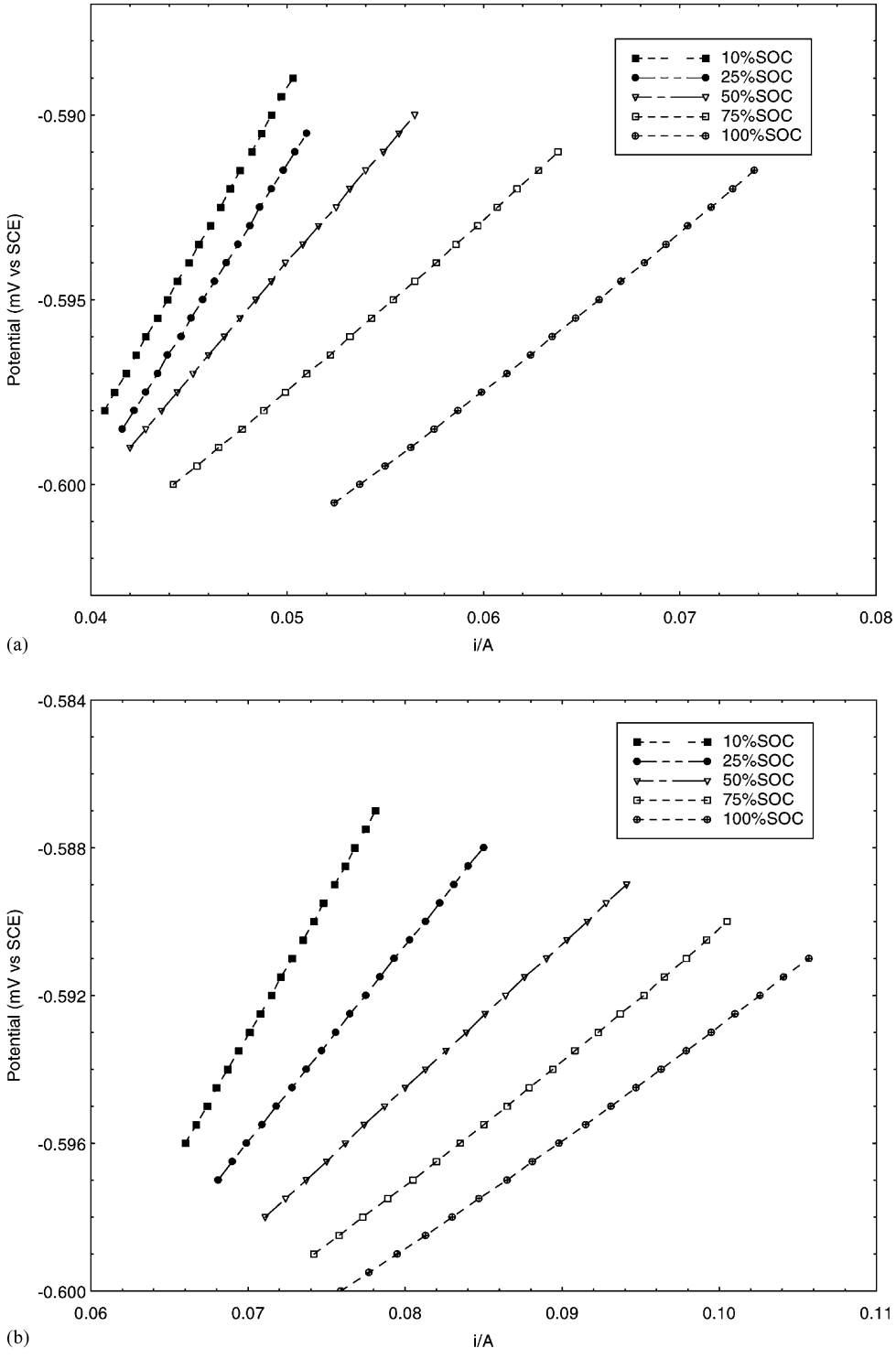

Fig. 9. Linear polarisation curves at various states-of-charge for: (a) untreated; and (b) etched alloy.

gas constant, T the absolute temperature. The symmetry factor (β) is determined from the slope of a plot of η versus $\log[i/(\exp(F\eta/RT) - 1)]$, i.e.

$$\eta = \frac{2.303RT}{\beta F}\log i_0 - \frac{2.303RT}{\beta F}\log\left[\frac{i}{\exp(F\eta/RT) - 1}\right] \quad (3)$$

The calculated exchange current densities are listed against the state-of-charge in Table 1. Comparing the exchange current density values, it can be seen that the surface-etched alloy shows a higher exchange current density than the untreated alloy. For fully-charged electrodes at maximum capacity, the value of the exchange current

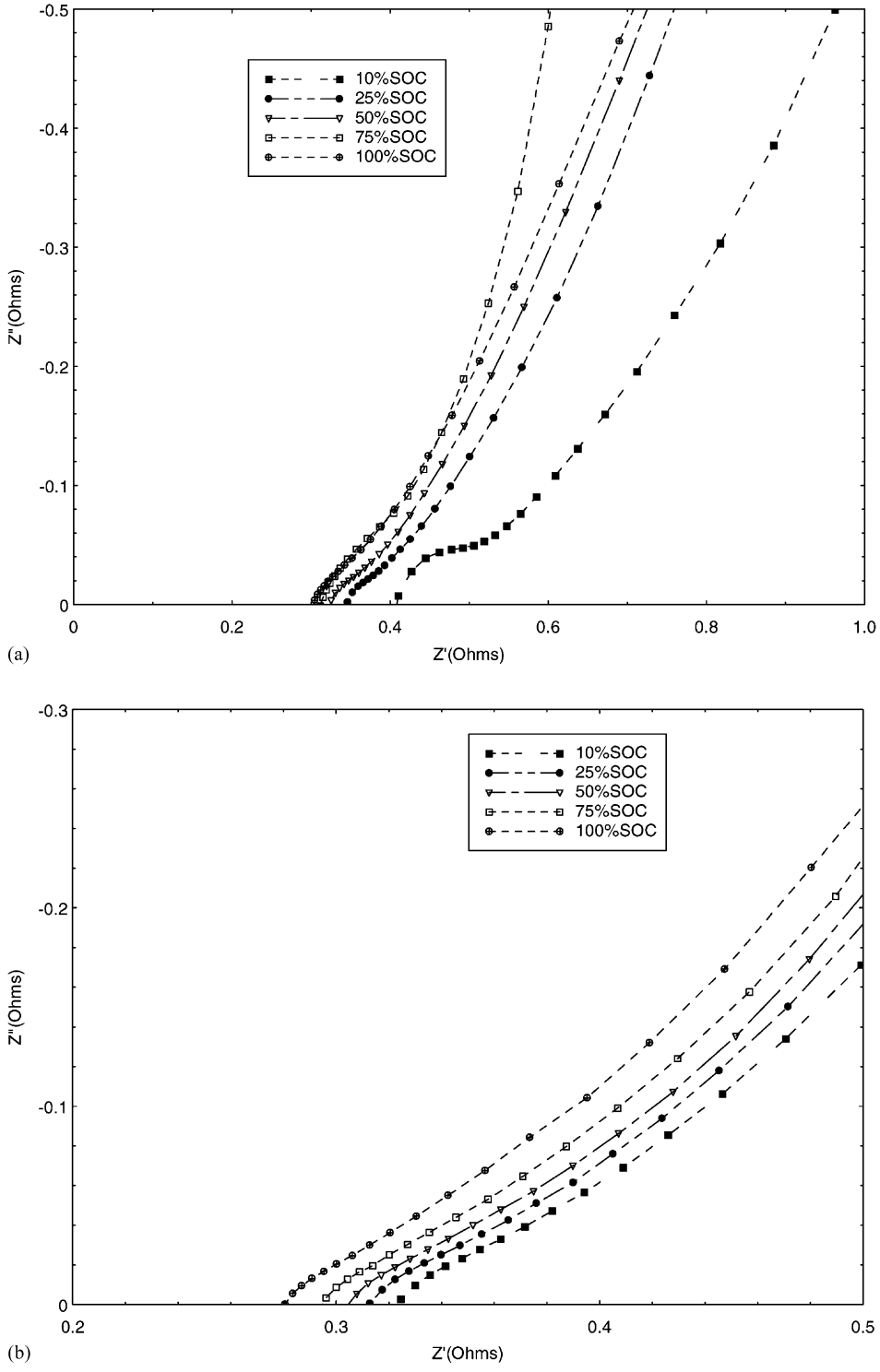

Fig. 10. Impedance curves at various states-of-charge for: (a) untreated; and (b) etched alloy.

density increases from 61.2 mA cm^{-2} for the untreated alloy electrode to 84.7 mA cm^{-2} for the surface-etched alloy electrode. The calculated polarisation resistance estimated for the untreated alloy is higher than that for the surface-etched alloy because the porous nature of the oxide surface on the etched alloy facilitates the charge-transfer reaction on the alloy surface.

In order to determine the symmetry factor, the linear polarisation curves of Fig. 9(a) and (b) are replotted according to Eq. (3). A linear relationship exists between η and $\log[i/(\exp(F\eta/RT) - 1)]$. The symmetry factor is found to be 0.85 for the untreated alloy and 0.84 for the etched alloy. The symmetry factor is not dependent on the hydrogen content of the alloy.

Table 2
Exchange current density (mA cm^{-2}) from ac impedance method

State-of-charge	For untreated alloy	For etched alloy
100	55.2	67.1
75	46.9	55.0
50	45.0	49.7
25	40.0	42.0
10	32.3	35.0

In order to study the effect of cycling on the kinetics of the etched alloy, polarisation was performed after the 150th cycle when the alloy capacity had decreased substantially. The resistance of the electrode was found to have increased and the corresponding exchange current density was only 12.9 mA cm^{-2} (a decrease from 84.1 mA cm^{-2} for the fully-charged alloy). This shows clearly that the etched alloy is susceptible to further oxidation and, hence, a decrease in exchange current density.

The hydriding reaction involves a charge-transfer step, followed by surface transition from adsorbed site on the electrode surface to the absorbed site in the near-surface region, and then diffusion of absorbed hydrogen from the near-surface into the bulk. Therefore, the contribution to the impedance is due to three steps which occur in series. Hence, ideally, the arc in the higher frequency region corresponds to the charge-transfer step, the second arc to hydrogen transfer between the adsorbed and absorbed states, and the arc in the low frequency range should represent the impedance for finite spherical diffusion in the electrode. At low diffusion constants (10^{-10} cm^2 s^{-1} or less), the arcs in high and middle frequency ranges disappear, and the arc in the low frequency range becomes larger to yield a linear region. This line is attributed to Warburg diffusion [17,18].

The ac impedance spectra of untreated and etched $TiMn_{1.6}Ni_{0.4}$ alloy at different states-of-charge were measured and are shown in Fig. 10(a) and (b), respectively. This hydride has a low diffusion coefficient of the order of 10^{-11} cm^2 s^{-1}. Hence, the two arcs in the high frequency range have almost disappeared and a prominent linear region due to the Warburg impedance can be clearly seen. At high states-of-discharge, when the charge-transfer resistance is higher, a semicircle can be seen. The charge-transfer resistance has been calculated at various states-of-discharge, and the exchange current density has been determined using Eq. (2) and is given in Table 2. For the etched sample, i_0 ranges from 67.1 to 35.0 mA cm^{-2}, while for the untreated sample it ranges from 55.2 to 32.3 mA cm^{-2}. The exchange current density is higher for the etched sample than for the untreated sample, which indicates higher activation for the etched alloy surface. The differences in the solution resistances for various states-of-discharge may be attributed to the impedance between the current-collector and the active material, and between the particles of the metal hydride alloy. On hydriding, hydrogen occupies the interstitial sites and volume expansion takes place. The latter results in better contact between the current-collector and hydride alloy, and between the hydride particles. Hence, the solution resistance increases on discharge.

4. Conclusions

The electrochemical properties of $TiMn_{1.6}Ni_{0.4}$ alloy treated with an etching solution have been compared with the untreated alloy. The results show that etching modifies the surface of the alloy and improves the activity of the alloy. The treated alloy displays higher discharge capacity and greater high-rate discharge capability than the untreated alloy. The etching treatment also improves the electrochemical reaction activity. The exchange current density values are higher for the treated alloy, as shown by polarisation and impedance measurements. Surface modification makes the oxide layer porous, and thus, it becomes active. The durability of untreated alloy is found to be better than that of treated alloy.

Acknowledgements

The authors wish to thank the management of the SPIC Science Foundation for support to conduct this research. The authors are also grateful to Dr. S Ramaprabhu, IIT Madras, for help in the preparation of the samples.

References

[1] Y. Moriwaki, T. Gamo, T. Seri, T. Iwaki, J. Less Common Met. 172–174 (1991) 1211.
[2] S.R. Kim, J.Y. Lee, J. Alloys Comp. 210 (1994) 109.
[3] T. Sakai, T. Hazama, N. Kuriyama, A. Hata, H. Ishikawa, J. Less common Met. 172–174 (1991) 1175.
[4] A. Zuttel, F. Meli, L. Schlapbach, J. Alloys Comp. 203 (1995) 235.
[5] M. Matsuoka, M. Terashima, C. Iwakura, Electrochim. Acta 38 (1993) 1087.
[6] J.J.G. Willems, K.H. Buschow, J. Less Common Met. 129 (1987) 13.
[7] B. Luan, N. Cui, H.K. Liu, H.J. Zhao, S.X. Dou, J. Power Sources 55 (1995) 197.
[8] S. Wakao, H. Sawa, J. Furukawa, J. Less Common Met. 172–174 (1991) 1219.
[9] D. Yan, G. Sandrock, S. Suda, J. Alloys Comp. 216 (1994) 237.
[10] S.R. Kim, J.Y. Lee, H.H. Park, J. Alloys Comp. 205 (1994) 225.
[11] W.K. Choi, K. Yamataka, S.G. Zhang, H. Inoue, C. Iwakura, J. Electrochem. Soc. 146 (1999) 46.
[12] D. Yan, S. Suda, J. Alloys Comp. 223 (1995) 28.
[13] A. Zuttel, F. Meli, L. Schlapbach, J. Alloys Comp. 209 (1995) 99.
[14] J. Chen, D.H. Bradhurst, S.X. Dou, H.K. Liu, J. Alloys Comp. 265 (1998) 281.
[15] M. Ciureanu, D.H. Ryan, J.O. Strom-Olsen, M.L. Trudeau, J. Electrochem. Soc. 140 (1993) 579.
[16] G. Zheng, B.N. Popov, R.E. White, J. Electrochem. Soc. 142 (1995) 2695.
[17] C. Wang, J. Electrochem. Soc. 145 (1998) 6.
[18] N. Cui, J.L. Luo, J. Electrochim. Acta 44 (1998) 711.